Modulation of Tremor Amplitudes by Tidal Stresses in Cascadia

Amanda Klaus

Manuscript for Master's project

Abstract

We recorded the 2010 and 2011 episodic tremor and slip events in Northern Cascadia on the Array of Arrays, a group of small-aperture seismic arrays on the northern Olympic Peninsula. We invert for amplitude at the tremor source and investigate the relationship between tremor amplitude and tidal stress, using a Cascadia-wide tidal loading model. We find enhanced tremor amplitudes at times of high shear stress. The amplitude modulation is strongest at the 12.4 h period tide, but we also observe a modulation associated with the 12 h and 23.9 h periods. Amplitudes are uncorrelated or anticorrelated with normal stress, which suggests low friction at the plate interface. The phase of the maximum amplitude roughly coincides with the phase of maximum slip rates and maximum numbers of tremor detections. We find a consistent offset between peak tremor amplitudes and peak tidal stress, assuming a friction coefficient less than 0.4, with peak amplitude preceding peak stress by about 1.5 hours.

1. Introduction

The anomalous GPS signals of slow slip events on the Cascadia subduction zone were discovered just over a decade ago [*Dragert et al.*, 2001]. Shortly thereafter, seismic signals associated with this slow slip event were discovered [*Obara*, 2002; *Rogers and Dragert*, 2003]. The seismic signal was termed non-volcanic tremor, and the whole event was termed episodic tremor and slip (ETS). ETS events have since been found in other subduction zones, notably Japan [*Obara*, 2002] and Mexico [*Payero et al.*, 2008], as well as the strike-slip environments of the Parkfield segment of the San Andreas fault [*Nadeau and Dolenc*, 2005] and the Alpine Fault in New Zealand [*Wech et al.*, 2012].

The seismic signal known as tremor is emergent, low in amplitude, and persistent over time scales ranging from minutes to weeks. At a single seismic station, the trace of tremor looks very much like noise. Unlike noise, however, tremor signals are coherent over stations many tens of kilometers apart.

ETS events happen throughout the entire length of the Cascadia subduction zone. In the southern segment, recurrence intervals are 10 ± 2 months, while in the central segment, recurrence intervals are 19 ± 3 months [*Brudzinski and Allen*, 2007]. The north segment, from Olympia, Washington to northern Vancouver Island, ruptures in an ETS that lasts for over a month and recurs every 14 months on average [*Brudzinski and Allen*, 2007]. Geodetic estimates of moment magnitude for ETS events in the northern segment range from 6.1 to 6.8 [*Schmidt and Gao*, 2010; *Szeliga et al.*, 2008].

Tremor is sensitive to very small stress perturbations. For example, bursts of tremor may be triggered by shear stresses on the order of 40 kPa caused by the passing surface waves from teleseismic events [*Rubinstein et al.*, 2007]. Tidal stresses may be an order of magnitude smaller than these surface wave stresses, and have not been observed to trigger tremor. However, tidal stresses have been observed to modulate tremor activity during an ETS event.

Tidal stresses have been observed to modulate numbers of tremor detections, or tremor "counts," in Japan, Cascadia, and on the San Andreas Fault. In Shikoku, Japan, the number of low frequency earthquakes (LFEs) detected rises and falls at a 12.3 hour period, consistent with the 12.4 M2 lunar tide [*Shelly et al.*, 2007]. During times when there is no tidal migration observed, tremor occurs primarily at high tide in Shikoku [*Ide*, 2010]. A modulation of tremor detections was seen in 12 events in Shikoku at periods of 12 and 24 hours [*Nakata et al.*, 2008]. That study used hourly tremor duration as a proxy for number of tremor detections and compared this quantity to a calculated Coulomb failure stress at the

centroid of the tremor event on the plate interface. The peak occurrence of non-volcanic tremor occurred before the peak Coulomb failure stress, but after the peak Coulomb stress rate [*Nakata et al.*, 2008].

Tidal modulation of tremor detections has also been observed in the creeping section of the San Andreas Fault. Both numbers of tremor detections [*Thomas et al.*, 2009] and numbers of LFE detections [*Thomas et al.*, 2012] are associated with increased right-lateral shear stress on the San Andreas.

Modulation of tremor amplitudes rather than tremor counts has received some attention in recent years. In Cascadia, tidal modulation of amplitudes was observed at several seismic arrays over three ETS events recorded on the Olympic Peninsula [*Rubinstein et al.*, 2008]. The spectra of these signals, which were not corrected for source-receiver distance, showed clear peaks at tidal periods, most strikingly at around 12.4 hours and 24 hours during ETS events. In contrast, the peak around 12 to 12.4 hours is insignificant outside of ETS events, while the 24 hour peak was much smaller. A plot of amplitude versus the phase of the 12.4 hour cycle showed a clear modulation during ETS events and a lack of modulation outside of ETS events.

Evidence for tidal modulation of amplitudes has also been seen on Vancouver Island. Lambert et al. [2009] defined tremor count as the number of seismic stations which record a given tremor waveform, and are expected to be proportional to tremor amplitude and size of the active area. Tremor count data in the tidal spectral band, from which a nontidal daily signal has been removed, shows a significant correlation with shear stress in the thrust direction, as well as a smaller correlation with normal stress.

Tidal modulation of slow slip has been inferred from stacking observations of five northern Cascadia slow slip events at six borehole strain meters [*Hawthorne and Rubin*, 2010]. Comparison with a tidal model revealed a modulation of slip rate at the M2 tidal period at the 99% confidence level. On average, the slip rate varies by up to 25% of the mean slip rate in sync with the shear stress of the 12.4 hour M2 tide. The maximum M2 shear stress and slip rate was found to be only a few degrees off from the maximum number of tremor detections.

The fact that tremor and slow slip are related is well-established. Exactly how they are related, however, is unclear. There is now a great deal of evidence that tremor is occurring on the plate interface and is directly related to slow slip [*Brown et al.*, 2009; *La Rocca et al.*, 2009; *Wech and Creager*, 2007], but the question of what physically is happening to produce tremor is still open. Comparison of tremor locations with slip inversions shows tremor originating behind the slip front, leading to the suggestion that tremor results from high slip rates on seismogenic asperities [*Bartlow et al.*, 2011]. Another possibility is that tremor is a signal of crack propagation at the slip front. It has been proposed that heterogeneities on the plate interface lead to “patches” with different frictional properties and different characteristic behavior [*Hirose and Obara*, 2010; *Ide*, 2012]. Some explanations have invoked fluids – the movement thereof itself as the source of tremor, or somehow enabling tremor and slow slip [*Kao et al.*, 2005; *Kato et al.*, 2010; *Rubin*, 2008]. Examining the relationship between tremor and tides may be able to shed light on these questions.

Several studies have looked to tremor amplitudes in order to estimate seismic moment release [*Kao et al.*, 2010; *Maeda and Obara*, 2009] or to determine scaling relationships [*Watanabe et al.*, 2007]. Much of the effort in investigating the tremor tide relationship, however, has focused on tremor counts rather than amplitudes. Studying tremor amplitudes is not simple. Tremor signals cannot be processed with conventional seismological methods; they require new methodologies [*Kao and Shan*, 2004]. Furthermore, when studying tremor on individual and often noisy stations, amplitudes barely exceed noise levels and observed dynamic ranges are small. In those cases, there is little to be gained from studying amplitudes, and tremor duration is a good proxy for seismic moment. However, with quiet stations and small-aperture arrays, the dynamic range of observable tremor amplitudes increases by a couple orders of magnitude.

In this study, we investigate the modulation of tremor amplitudes in Cascadia by tidal stresses. We recorded the 2010 and 2011 Cascadia ETS events on the Array of Arrays, an experiment of small (~1 km

aperture) arrays on the northern Olympic Peninsula. The high signal-to-noise ratio of these arrays allows for new and improved analyses of Cascadia tremor data. We perform an inversion for tremor amplitude at the source location and analyze the relationship between tremor amplitudes and tidal stresses. We find strong evidence for modulation of tremor amplitudes by the tides, particularly by the shear stress of the 12.4 hour M2 tide. The limited influence of the tidally-generated normal stress suggests low friction at the plate interface. We also find a ~1.5 hour offset between peak amplitude and peak tidal stress, which is challenging to interpret, but also has been seen by other researchers.

2. Calculation of Tremor Amplitudes

2.1. Data

Tremor amplitudes are generated from waveforms recorded on the Array of Arrays (AofA), CAFE arrays Big Skidder (BS) and Price Lake (PL), and individual CAFE stations W020, W040, and W060 (Figure 1). Each AofA array has an aperture of about 1 km, and comprises 10-20 short-period three-component velocity seismometers. These stations recorded both the August 2010 and August 2011 ETS events, as well as several small inter-ETS events in 2010.

Signal-to-noise ratio is generally poor in recordings of tremor events on account of the low seismic amplitude of tremor. The Array of Arrays significantly improves signal-to-noise ratio by allowing for stacking across the array.

Tremor locations are determined using a waveform envelope cross-correlation method [*Wech*, 2010; *Wech and Creager*, 2008]. The tremor location catalog uses real-time data from the Pacific Northwest Seismic Network (PNSN), Pacific Geoscience Centre, and Plate Boundary Observatory (PBO) seismometers. Locating tremor is thus independent of the amplitude calculations, which are based on quiet stations without telemetry.

2.2 Calculating amplitudes

For each station, the seismograms are filtered from 1.5 to 3 Hz, and envelopes are made for the north channel of each station. To stack over arrays, we take the median of all the stations at each time point. Because we are working with the low end of the tremor frequency band and our apertures are small, we do not have to do any time-shifting in the stack for account for the different arrival times across the small array.

At this point, we have an average amplitude for every five minutes at each station. For each five-minute-window where tremor is detected, we calculate the amplitude corrected for geometric spreading and attenuation, A_i, as follows:

$$A_i = x_i \cdot R^{-1} \cdot e^{\pi f_c R / Q V_S}$$

where x_i is the amplitude at the station of the ith five-minute window, R is the source-receiver distance, f_c is the center frequency, Q is the quality factor for shear wave attenuation, and V_s is the shear-wave velocity. Source-receiver distance is calculated as a straight line, simplifying the geometric spreading calculation. Tremor locations are assumed to be on the plate interface, using the contours of McCrory et al. [2004]. We use values of f_c = 2.0 Hz, Q = 180, and V_s = 3.5 km/s.

After this correction, we perform a least-squares inversion of the log of corrected amplitude for the log of amplitude at the source and for site corrections. This results in a single measurement for relative amplitude at the tremor source for each five-minute window in which tremor is detected.

2.3 Tidal model

We use the tidal stress model of Hawthorne et al. [2010]. The model was created using the loading software SPOTL [*Agnew*, 1997], which calculates strains at Earth's surface from solid earth tides and ocean tide loading. In this model, solid earth tides are only computed at the surface. This is considered valid because the solid earth tides have little spatial variation and are smaller than ocean loading stresses [*Hawthorne and Rubin*, 2010]. Ocean tide stresses, in contrast, are computed at the plate interface instead of at the surface [*Hawthorne and Rubin*, 2010], using the plate interface model of McCrory et al. [2004]. Tides included in this model are the M2 (12.4 hour period), S2 (12.0 h), N2 (12.65 h), K1 (23.9 h) and O1 (25.9 h) tides. These are the highest amplitude and hence the most influential tidal stresses. There are other tidal periods, but they are omitted from the model as unnecessary; their amplitude is small, and they account for little of the variance in the tidally-induced strain rate [*Hawthorne and Rubin*, 2010].

The resulting model calculates normal stress and shear stress in the slip direction on the plate interface. Normal stress is tension positive, so both positive normal stress and positive shear stress would be expected to enhance slip on the interface. We use a slip direction of N55°E, based on plate convergence vectors of McCaffrey [2007] and roughly consistent with tremor polarization measurements [*Wech and Creager*, 2007].

3. Results of Analysis

3.1 Spectra of Amplitudes

The spectra of tremor amplitudes for both the 2010 and 2011 ETS events show strong evidence for tidal modulation (Figure 2).

For both years, the largest peak occurs within 0.2% of the 12.42 hour M2 tidal period, consistent with previous work suggesting that the 12.4 hour tide is the most important for tidal modulation [*Hawthorne and Rubin*, 2010; *Rubinstein et al.*, 2008; *Shelly et al.*, 2007]. A smaller peak is consistent with the 12 hour tide, with a 0.01% error in this peak in the 2010 spectrogram. A large peak at the 23.9 hour O1 tide (<0.5% error) is also evident. Caution must be used in interpreting this peak, as cultural noise has a 24 hour periodicity, peaking in the day and falling to a minimum at night. However, there is strong evidence that this peak is related to the tides rather than to noise. Firstly, the Array of Arrays stations are in remote locations with relatively low cultural noise levels. Secondly, Rubinstein et al. [2008] compared spectra of seismic records at five different seismic stations for time periods with and without tremor. They found that the ~24 hour peak was significantly lower at even the noisiest arrays when tremor was not active.

The spectra, therefore, show significant energy at tidal periods of 12.4 and 23.9 hours, and possibly also at 12.0 hours. This strongly suggests a tidal modulation of tremor amplitudes. However, these spectra do not tell us *how* tremor amplitudes are related to tidal stresses. To better understand this relationship, we compare amplitude records with modeled tidal stresses.

3.2 Constraining study areas with tidal model

Both phases and amplitudes of predicted tidal stresses vary dramatically over the ETS source region in Cascadia, particularly in the northern section that we focus on, largely due to the complex

network of waterways. Ocean tides in the Strait of Georgia, for example, are nearly 180° off from tides in the open ocean, leading to dramatic phase shifts over a relatively small spatial extent. This poses a difficulty in attempts to compare tremor amplitudes to tides. If we look at the entire ETS region, it is difficult to see any relationship. Tremor in different locations may be responding to tides in a consistent way, but responding to very different tidal stress regimes, so its response fails to look consistent or coherent.

A solution to this issue is to use the tidal model to limit the study to areas over which the tidal stresses behave nearly identically, particularly with respect to phase. To do this, we generate time series of the modeled tidal stress on the plate interface at many grid points. We then select a reference point, cross-correlate the tidal stress time series at all grid point with the time series at the reference point, and define the edges of our "polygon of interest" as the limits of a certain cross-correlation value at zero lag.

Polygons used in this study are shown in Figure 1. Their edges are at a correlation value of 0.93, meaning that tidal stresses within the polygon correlate with each other at a value of 0.93 or higher. This value was chosen in order to ensure coherent tidal stresses while allowing the polygon to be large enough to contain sufficient data for analysis.

3.3 Comparing amplitude and stress in time

By using the detailed tidal model, which provides tidal stresses at any point on the plate interface at any time, we can directly compare the amplitude time series with the changing tidal stresses. This allows for detailed exploration of the relationship between these two quantities despite the complicated environment.

In Figure 3, we compare tremor amplitudes with tidal stresses in each of two polygons. These polygons are shown in Figure 1, and are defined as described in section 2.4. The amplitude time series in Figure 3 have been smoothed with a running average over three hours to approximate a low-pass filter, as we do not expect high-frequency fluctuations in amplitude to be explicable by tidal stresses. The tidal stresses, which are calculated at the polygon reference point, are Coulomb stresses, defined as

$$\sigma_C = \sigma_S + \mu\sigma_N$$

where σ_C is Coulomb stress; σ_S is shear stress in the slip direction; σ_N is the stress normal to the plate interface, and is tension-positive; and μ is the friction coefficient. Figure 3 uses a friction coefficient μ = 0.1. Comparison of these figures shows a remarkable similarity between the amplitudes and tidal stresses. For the most part, peaks of tremor amplitudes in this frequency band nearly coincide with the peak tidal stresses.

We can test many values of μ to see if a certain value best fits the amplitude data. Figure 4 shows the correlation coefficient between amplitude and tidal stress for values of μ ranging from 0 to 1 on the Olympic Peninsula and Vancouver Island. In both cases, the highest correlation occurs at μ = 0, meaning that amplitudes correlate best with shear stress alone, although values up to about μ = 0.2 produce statistically significant correlations between amplitude and stress.

3.4 Phase-amplitude relationship

In investigating the ideal value of μ, we compared the correlation coefficients without considering any lag. However, introducing a time shift is necessary to maximize the correlation between the two time series. The highest correlation between tremor amplitude and stress, for μ ranging from 0 to ~0.3, occurs with maximum amplitude leading by 1 to 2 hours (Figure 5). This means that the maximum amplitude occurs about one hour before the maximum tidal stress.

This is borne out by plots comparing the average tremor amplitude to the phase of the 12.4 hour tide's shear component (Figure 6). On average over the study area, the maximum average amplitude occurs around a phase of 40° to 65°, corresponding to a lead time of 1.25 to ~2 hours. The fact that the peak amplitude precedes the peak stress is difficult to explain. It could mean that tremor is encouraged at some threshold value rather than at the maximum, or it could mean that amplitudes are responding to the stress rate rather than to the stress.

A phase-amplitude comparison with the stress rate for the 12.4 hour shear stress does show the peak stress rate preceding the peak tremor amplitude by 0 to 2.5 hours (Figure 7). Cross-correlating tremor amplitudes and shear stress rate in the same manner as in Figure 5 shows an amplitude lag of 0.9 to 1.8 hours. It is not clear why amplitude should peak an hour or more after the stress rate does, but some possibilities are discussed in Section 4.3.

3.5 Possible spatial variation in friction

In sections 3.3 and 3.4, we showed that low values of the friction coefficient μ best explain the variations in tremor amplitude. These values of μ are averages over a large area. We investigate whether we can constrain μ over smaller spatial scales.

First, we make a 5 km grid over the study area, and calculate a time series of tidal Coulomb stress (μ = 0.1) for each grid point. We select a grid point as a reference and calculate the region on the slab interface that is within 25 km of the reference and such that the time-history of Coulomb stress correlates above 0.93 with respect to the coulomb stress at the reference point. We then select all the tremor locations that lie within that region This produces, for each reference point on the grid, a set of tremor amplitudes that are nearby and subject to the same tidal stresses at the reference point.

Next, for each grid point, we calculate the correlation coefficient between the amplitudes of tremor associated with that reference point and the tidal stress at the reference point for values of μ from 0 to 1, as in Figure 4. The time of each tremor amplitude measurement is shifted forward in time by 1.5 hours in order to measure the correlation between peak amplitude and peak stress.

The resulting 'best' μ – defined as the μ which produces the highest correlation between tremor amplitude and Coulomb stress – is shown in Figure 8b. Figure 8a shows the smallest value of μ that correlates within the 95% confidence limits of the value for the best μ; Figure 8c shows the largest value of μ within those same limits.

A value of μ = 0 as the lower bound on μ, with acceptable values of μ ranging from 0 to 0.2, produce the best correlation in most locations. The expection is a patch at the south end of our study area, where the lower bound in μ can be as high as 0.25, and the best μ values are as high as 0.41. This area seems to prefer a higher value of μ, suggesting some structural difference, and indeed, the seismic waves speeds in the crust immediately above the plate interface in this area below the core of the Olympics are anomalously slow [*Preston et al.*, 2003]. However, the stressing is also different in this region. In much of the study area, normal stress is roughly out of phase with shear stress and is much larger, so that the Coulomb stress time series becomes extremely similar to the normal stress for values of μ greater than 0.4 or so. In this southern section, though normal and shear stress are out of phase, normal stress is not very much larger than the shear stress. Here, adding in moderate values of μ produces a stress time series whose phasing is intermediate between that of the shear and normal stresses. The maximum tremor amplitudes occur roughly an hour or two before the peak shear stress. Because peak amplitude leads peak shear stress by about 1.5 hours, this puts the Coulomb stress time series right in phase with the tremor amplitudes. This is the only part of the study area with this stressing behavior. We believe that the suggested high value of μ is due to a coincidence of the stressing regime rather than an actual change in frictional properties. It should be noted that μ = 0 still produces a statistically significant correlation here.

It is also notable that regions where μ is not tightly constrained by this method correspond almost exactly to the regions where normal stress is very low or shear stress is very high (Figure 9). Because of this, even fairly high values of μ produce a Coulomb stress time series that is very similar to the shear stress time series. There is simply not enough change to the stress to allow μ to be constrained. This is especially true in the northwest corner of the grid, where normal stress is also in phase with shear stress. In that area, adding in even very large amounts of normal stress does not meaningfully change the phase of the shear stress, so the correlation with the amplitude time series cannot change much.

3.6 Constraints on the slip direction

In Section 3.5, we find correlation coefficients between tremor amplitudes and tidal stresses over the plate interface. We now address the question of whether a particular slip direction will maximize the correlation. To do this, we perform an analysis similar to that described in Section 3.5 for a given convergence direction, but only for μ = 0.1. We also include the 1.5 hour time shift. Then, for each convergence direction, we estimate how well this convergence direction fits by averaging the correlation coefficients of all the grid points which have at least 40 data points contributing to the correlation measurement.

The result is a fairly flat positive correlation between 10° and 80° from north (Figure 10). This analysis is only able to rule out convergence directions less than 10° and greater than 100°. Considering that convergence directions are generally estimated to be 50° to 60°, this is not much of a constraint. It does show that the expected convergence directions are valid, and that the choice of convergence direction within the expected range makes little difference to our results. This also affirms that analyses that use the dip direction as the slip direction is a reasonable approximation.

3.7 Tidal Sensitivity

A negative correlation between tidal sensitivity and tremor duration has been found in Nankai, Japan; northern Cascadia; southern Chile; and Mexico [*Ide*, 2012]. We modify this calculation in order to investigate whether there is a relationship between tidal sensitivity and tremor amplitude in Cascadia.

We define tidal sensitivity to the 12.4 hour M2 tide as follows:

$$s = \left| \sum_{i=1,..N} A_i \exp(i2\pi t_i / T) \right| / \sum_{i=1,..N} A_i .$$

where A_i is ith amplitude measurement, t_i is the time that A_i occurs, T is 12.4206 hours, and N = 100. For each point on a 5 km grid, 100 tremor detections within a 10 km radius are used in the calculation. We use tremor from both the 2010 and 2011 events. If there are more than 100 detections within 10 km, we use 100 tremor events that are as evenly spaced in time as possible.

A sensitivity value of s = 1would mean that tremors happened exactly every 12.4 hours, while a sensitivity value of 0 would mean that tremor was distributed randomly with respect to this period.

We find sensitivity values ranging from nearly 0 to 0.5, most measurements less than 0.3 (Figure 11). This is consistent with the finding that Cascadia has relatively low tidal sensitivity [*Ide*, 2012], meaning that although there is more tremor at certain times in the tidal cycle, there is also ample tremor that does not have a 12.4 hour periodicity.

In comparison with one another, the sensitivity maps and the median amplitude maps appear to be anti-correlated (Figure 11). In fact, there is a negative correlation between tidal sensitivity and median amplitude, although the correlation is only significant at the 1σ level.

Unfortunately, our results cannot be directly compared to Ide's [2012]: his improved location catalog is limited mainly to Vancouver Island. Although our tremor catalog extends onto Vancouver

Island, our Array of Array-derived amplitudes are most robust on the Olympic Peninsula and are less trustworthy moving north on Vancouver Island, so our sensitivity and amplitude comparison is limited to a different location on the subduction zone. However, our range of sensitivities is consistent with Ide's results [2012]. Relating amplitudes to duration is not simple, but has important implications for the dynamics of tremor, and will be discussed further in section 4.4.

4. Discussion of results

4.1 Amplitude modulation by tidal stress

These results show a clear and strong modulation of tremor amplitudes by tidal stresses. Though tidal modulation of tremor amplitude has been seen in Cascadia before [*Rubinstein et al.*, 2008], this work represents a significant improvement. Recording tremor on multiple arrays during an ETS event has improved the signal-to-noise ratio and has allowed us to invert for amplitude at the tremor source. We both see peaks around the 12.4 and 23.9 hour tidal periods. Our peaks, however, are much more well-constrained, being only a third the width. We also see a clear peak at 12.0 hours, which could not be seen in Rubinstein et al.'s [2008] results due to the width of the 12.4-hour peak.

We also confirm the counter-intuitive observation that higher tremor amplitudes are associated with higher water tides [*Rubinstein et al.*, 2008], which in turn corresponds to increased compressive normal stress on the plate interface that should inhibit slip. However, because the shear stress encouraging slip in our study area is generally roughly anti-correlated with the normal stress that encourages slip, we infer that the shear stress is the more important factor, even though the shear stress is often smaller in amplitude. The inferred small values of the friction coefficient μ diminish the importance of the normal stress relative to the shear stress. We also find that high tremor amplitudes are encouraged by high shear stress in the same way as tremor detections and slow slip rates.

4.2 Low μ

We find the best correlation between tremor amplitude and tidal Coulomb stress time series for very low values of friction (μ). A value of μ = 0 to 0.1 produces a statistically significant ($\geq 2\sigma$) correlation between tremor amplitudes and Coulomb stress for both ETS events and in both of our polygons (Figures 4, 5, 9). This was tested over smaller polygons and the results were the same.

Shear and normal stress are nearly 180° out of phase over most of the study area, such that loud tremor occurs when shear stress is encouraging tremor and when normal stress is discouraging tremor. When shear stress is at a maximum, the normal stress is at its most compressive. Conceptually, this means that when the shear stress that would enhance slip is greatest, there is increased normal stress that should be 'clamping' the plate interface and inhibiting slip. The fact that we see an encouragement rather than an inhibition of tremor at these times means that the normal stress is having little to no effect. For this to be possible, effective normal stress must be low, likely due to high pore pressure [*Hawthorne and Rubin*, 2010]. Other work on the tremor-tide relationship has noted that most of the tidal influence can be explained by the shear stress [*Hawthorne and Rubin*, 2010; *Lambert et al.*, 2009; *Thomas et al.*, 2009; *Thomas et al.*, 2012]. The triggering of tremor by kPa-scale perturbations from teleseismic Love waves also supports the interpretation of low effective normal stress [*Gomberg et al.*, 2008; *Rubinstein et al.*, 2007].

There already exists ample evidence for low friction at the Juan de Fuca plate interface. Tomography in Cascadia is consistent with elevated pore fluid pressure at the Juan de Fuca plate interface [*Audet et al.*, 2009; *Audet et al.*, 2010]. In Japan, tomography also shows high pore fluid pressure

at the plate interface [*Shelly et al.*, 2006], suggesting that near-lithostatic pore pressure may be a fundamental feature of tremor-generating interfaces [*Peng and Gomberg*, 2010].

Using a different methodology – in effect, by making hundreds of small polygons rather than two large ones – we do find that values up to $\mu = 0.4$ maximize the correlation in one area (Figure 5). However, values of $\mu = 0$ to 0.1 produce 95% significant correlations at all points in the study area, and the high μ values may be spurious.

4.3 ~1.5 Hour lead

As shown in section 3.3, the peak tremor amplitude precedes the peak stress by 1 to 2 hours. This is true for both the 2010 and 2011 ETS events, and true on both the Olympic Peninsula and Southern Vancouver Island. This result is similar to the finding that peak slip rate leads peak stress by about one hour [*Hawthorne and Rubin*, 2010]. Importantly, this demonstrates that high slip rates are associated with increased tremor detections and higher tremor amplitudes, confirming that tremor amplitude likely carries information about the amount of slip that is occurring.

However, caution must be used in comparing both of these results to the phase of the stress, because we use the same tidal stress model and there are many factors that introduce uncertainty into the tidal stress model. Any errors or inaccuracy in the calculation of stress at depth or in assumptions about mechanical properties could change the result. The convergence direction used has a negligible effect on the calculated tidal stresses, but the strike and dip of the plate model does have a significant effect. With San Andreas tremor, it was possible to find the optimal strike because it could be assumed that the fault was vertical and planar [*Thomas et al.*, 2012]. Unfortunately, the Juan de Fuca subduction interface is considerably more complex; dip changes with depth, and both strike and dip change significantly around the large plate bend north of the Olympic Peninsula. Relying on the smooth plate model of McCrory et al. [2004] is therefore the best choice, but any uncertainties in that model can affect our results.

A lag or lead between tremor activity and stress has, however, been observed in other locations independently. In Japan, peak tremor activity appears to occur “a few hours” before peak Coulomb stress but a few hours after peak stress rate [*Nakata et al.*, 2008]. They explain this time shift using a rate-and-state friction model, wherein the tremor activity depends on the Coulomb stress rate combined with the rate-and-state behavior.

At Parkfield, LFE activity is skewed in the other direction, with the greatest number of detections sometimes occurring about half an hour after maximum shear stress [*Thomas et al.*, 2012]. Possible explanations for this observation include LFE activity being initiated at peak stress but continuing on after; a threshold failure model; and normal stress fluctuations.

In the case of our observed 1.5 hour lead between tremor amplitude and stress amplitude, it is possible that tremor amplitude is enhanced at a certain threshold value of stress regardless of the maximum value of the stress, or it could be that high amplitudes are triggered with rate-and-state behavior by the peak stress rate. Uncertainties in the tidal stress model prevent us from being confident in this result. The possibility remains that it is not real. However, the fact that a similar result has been found in Japan suggests that this observation could be real [*Nakata et al.*, 2008]. More work on the tremor-tide phase relationship in Cascadia as well as in other locations is needed to confirm or deny this result.

4.4 Tidal sensitivity

Our method for calculating amplitudes, unfortunately, does not allow us to produce independent measures of tremor duration using the method of Ide [2012], which calculates the amount of time in a five-minute window where the amplitude is greater than half of the maximum amplitude in the window.

There are two potential explanations for the anticorrelation between tidal sensitivity and tremor amplitude.

The first is that our results are entirely consistent with Ide's [2012], which would mean that high tremor amplitude is linked to high tremor duration. Ide explains longer-duration tremor as tremor occurring in an area that is low in asperities, making it able to slip for a long time without any force stopping it; the fact that is already being driven by other forces makes it less sensitive to tides. This could mean that high tremor amplitude means that a larger area of the plate interface is slipping, with the possible corollary of association with greater slip. The fact that we see high tremor amplitudes at the same time that high strain rates, and hence higher slip rates, occur on the plate interface [*Hawthorne and Rubin*, 2010] supports this hypothesis.

The second possibility is that high tremor amplitude is the result not of high slip or of larger rupture areas, but instead is a result of slip on asperities that produce more seismic radiation. This might mean that higher amplitudes were instead associated with shorter duration tremor.

5. Conclusion

We see a clear modulation of tremor amplitudes by tidal stresses in the 2010 and 2011 ETS events recorded in the high quality Array of Arrays dataset. When shear stress is high, tremor amplitudes are enhanced by about 25% relative to the mean. The highest amplitudes occur slightly before the maximum stress, but after the maximum stress rate. This apparent offset could be merely a result of uncertainties in the model: errors in the plate model or in the loading calculation, for example, can change the phase of the tidal stress on the plate interface. However, other observations of time lags between tremor and tidal stress suggest that it could this offset may be real. Possible explanations for the phase shift a rate-and-state governed response to the stress rate [*Nakata et al.*, 2008] or tremor response at some threshold stress value [*Thomas et al.*, 2012].

Both the phasing of the modulation and the degree of modulation are consistent between tremor amplitudes and strain rates [*Hawthorne and Rubin*, 2010]. This reinforces that tremor is the seismic signal of slow slip, and confirms that tremor amplitudes convey information about slow slip activity.

The 12.4 hour ocean tide is the most important tide for modulating tremor amplitudes, consistent with previous work [*Hawthorne and Rubin*, 2010; *Rubinstein et al.*, 2008; *Shelly et al.*, 2007]. We also see tremor amplitude modulation at 12.0 and 23.9 hour periods. We find that the shear stress appears more important than the normal stress in modulating tremor amplitudes. The normal stress is often uncorrelated or anticorrelated with tremor amplitudes, while shear stress correlates with tremor amplitudes.

Tremor amplitudes are enhanced by high shear stress even at times when increased normal stress is expected to inhibit tremor. Tremor amplitude time series correlate best with Coulomb stress time series with friction coefficients of less than 0.4, in general. Friction coefficients of $\mu = 0$ to 0.1 produce correlations between tremor amplitude and Coulomb stress that are significant to at least the 95% confidence level at all studied locations. Spatial variability in tidal sensitivity suggests some heterogeneity in frictional properties, but overall, the observations support the interpretation that friction on the plate interface is very low during episodic tremor and slip events.

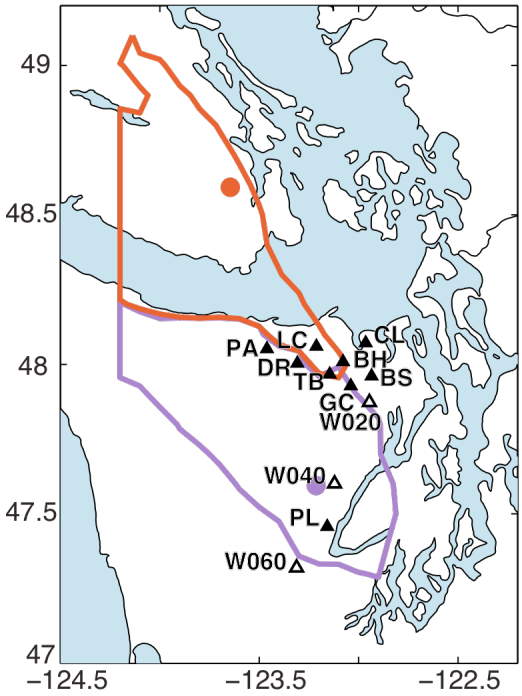

Figure 1. Locations of arrays (solid triangles) and single stations (hollow triangles) used. The polygons describe areas of consistent tidal stress on the plate interface, as described in Section 2.4. The purple (southern) polygon is the Olympic Peninsula polygon. The orange (northern) polygon is the Vancouver Island polygon. The dots of the corresponding colors are the polygon reference points.

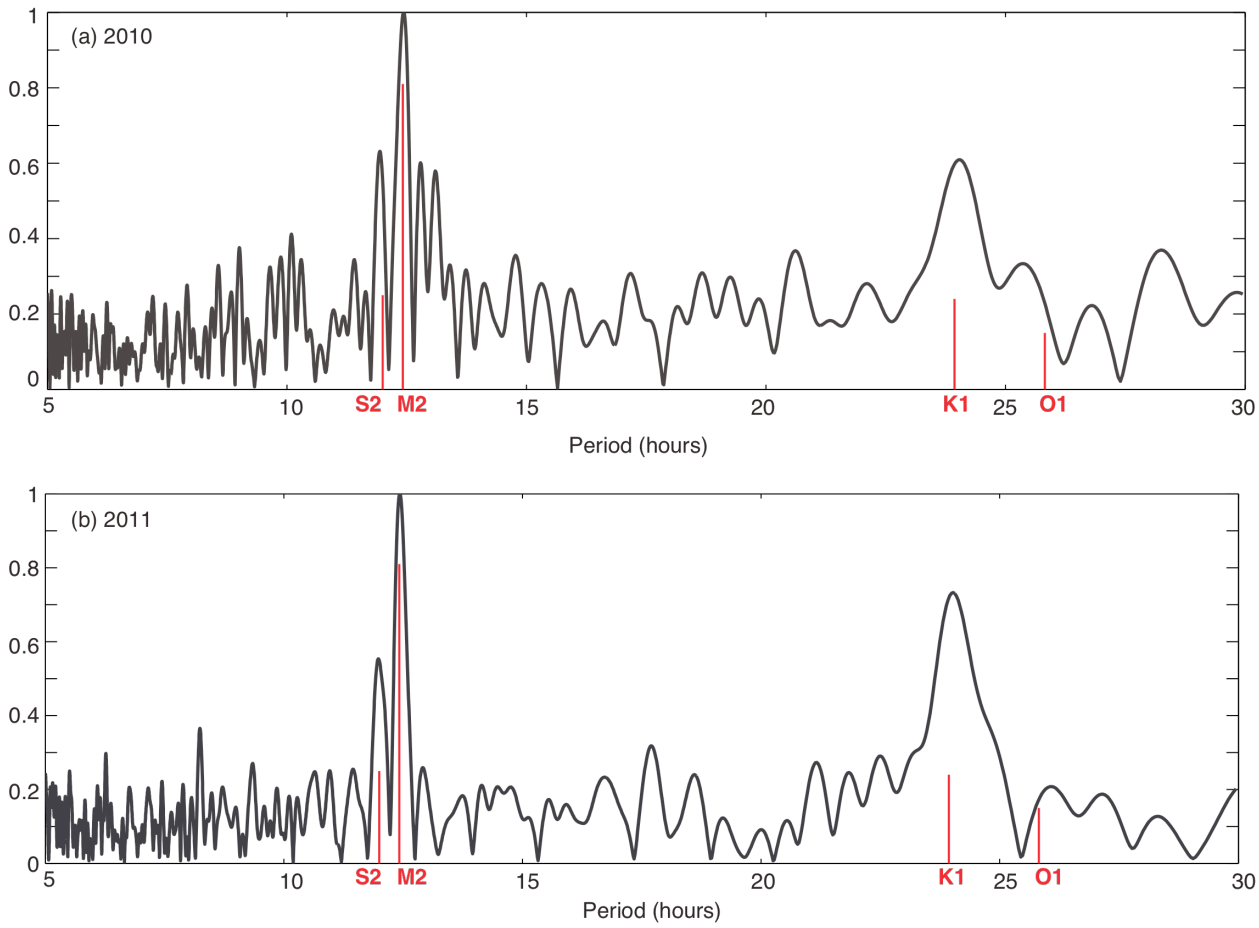

Figure 2. Amplitude spectra for two ETS events: (a) August 8 through September 8, 2010, and (b) August 1 through September 4, 2011. Red lines show the S2 (12.0 h), M2 (12.4 h), K1 (23.9 h), and O1 (25.6 h) tidal periods. The lines are scaled to the average amplitude of that tide.

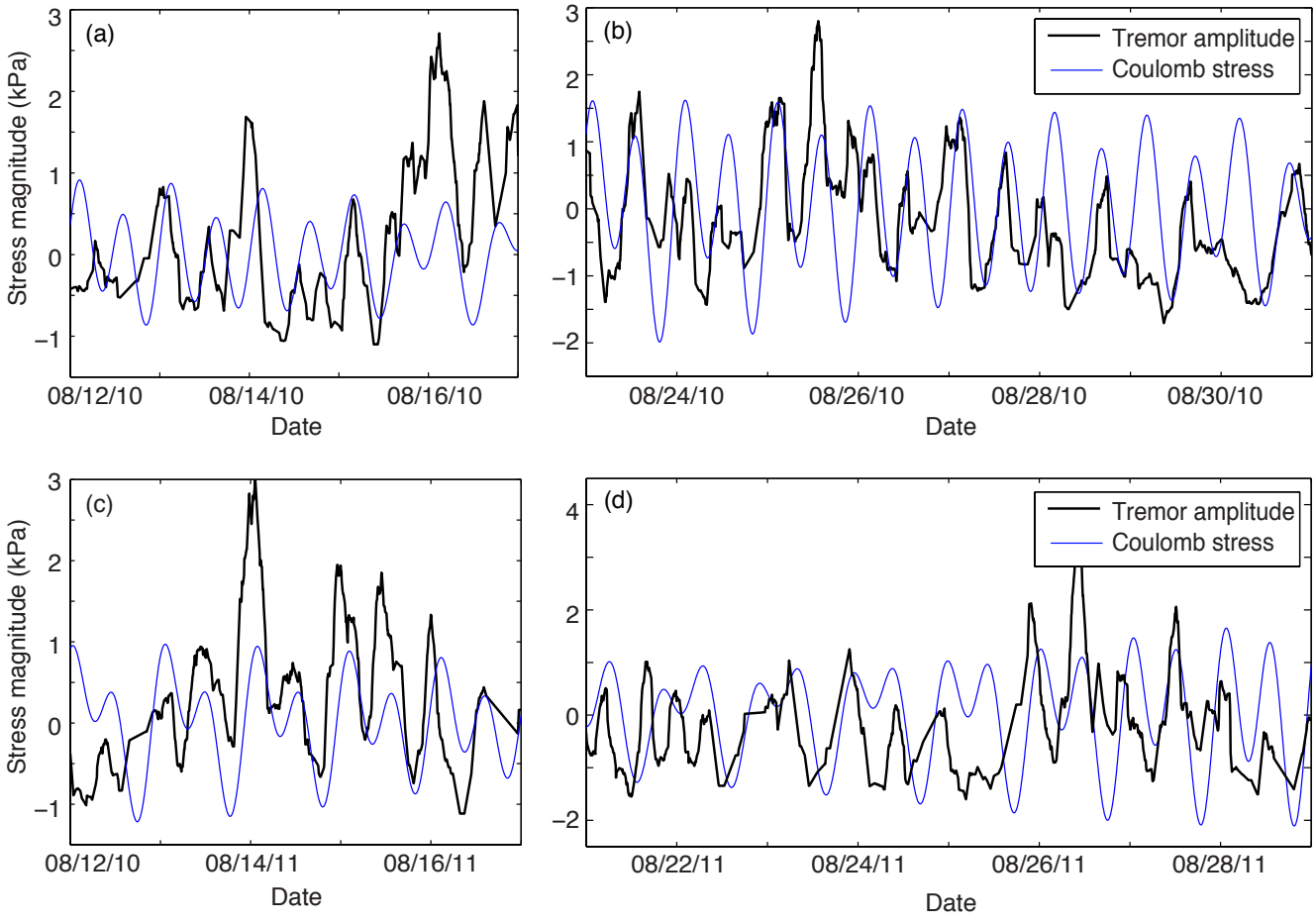

Figure 3. Comparison of tremor amplitudes (black) and tidal shear stress at polygon reference point (blue), for (a) Olympic Peninsula polygon, 2010; (b) Vancouver Island polygon, 2010; (c) Olympic Peninsula polygon, 2011; (d) Vancouver Island polygon, 2011. Amplitudes have been smoothed with a 3-hour running average to facilitate visual comparison in a tidal band. Each figure is limited to times when most of the tremor was in the respective polygon.

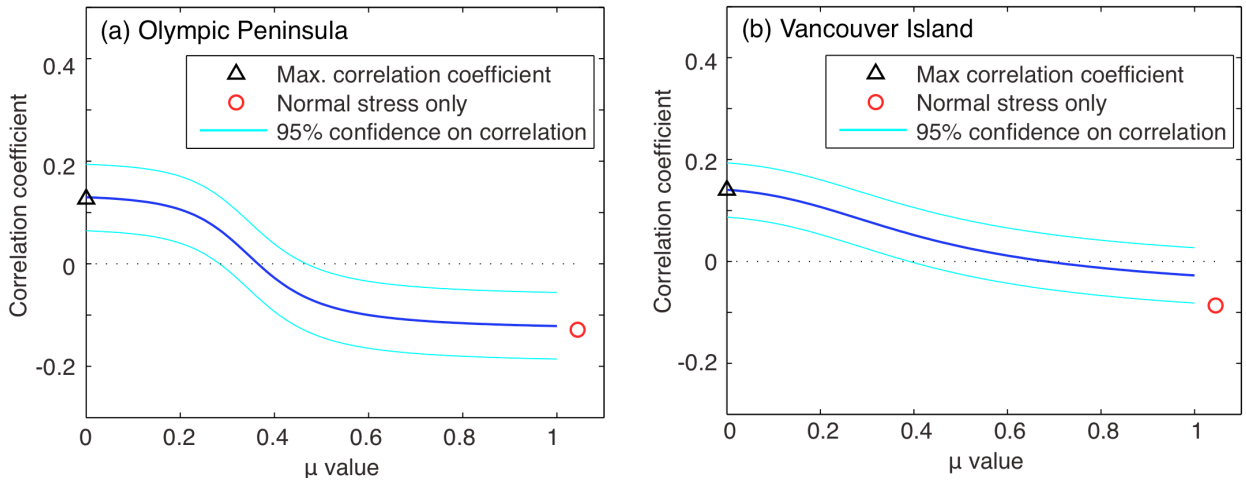

Figure 4. Correlation coefficient between tremor amplitudes (2010 and 2011 ETS events) and tidal Coulomb stress at polygon reference point for (a) Olympic Peninsula and (b) Vancouver Island, for values of μ ranging from 0 to 1. The bounding lines show the 95% confidence limits on the correlation coefficient. The red dot shows the correlation between tremor amplitudes and normal stress only.

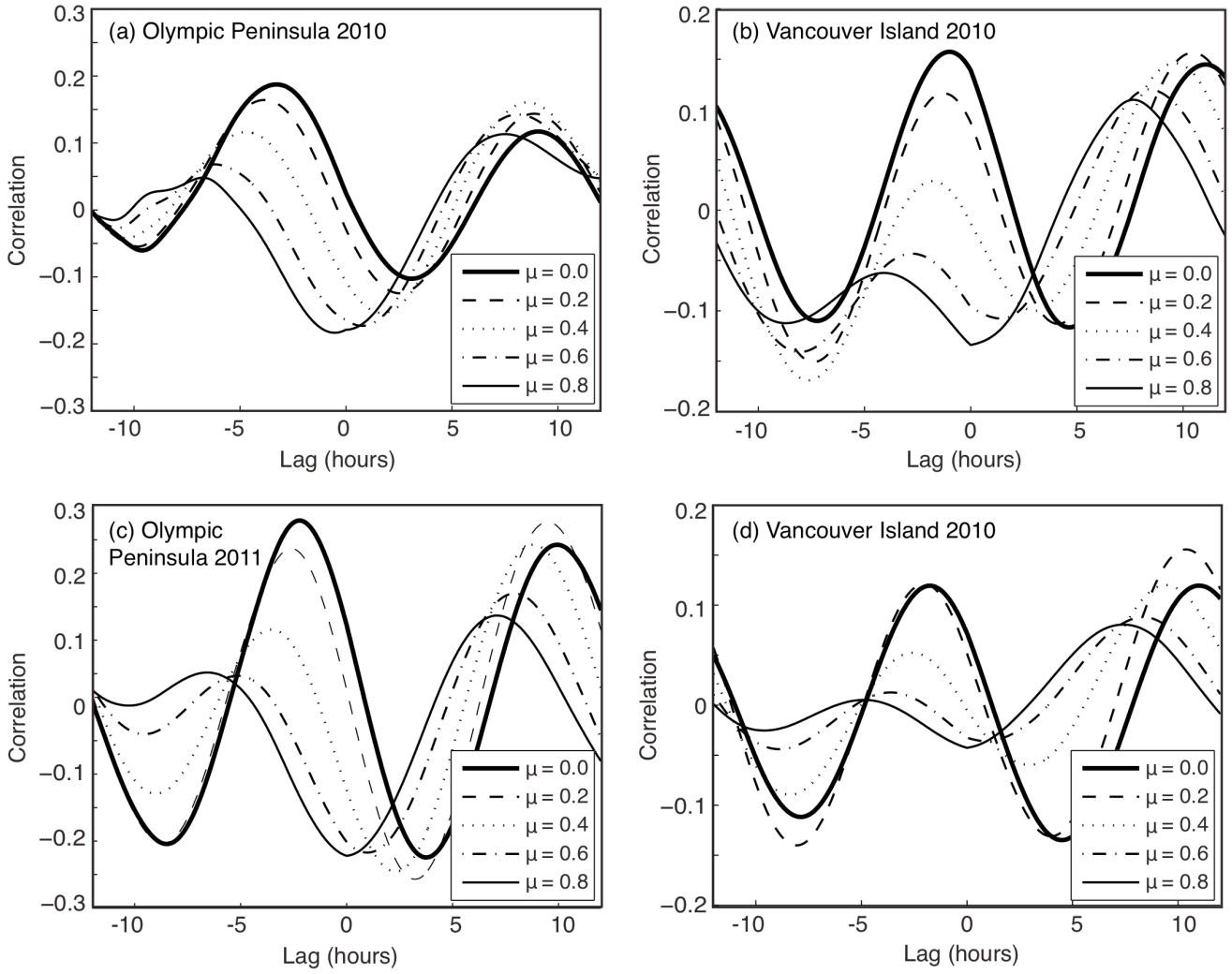

Figure 5. Cross correlation between tremor amplitude time series and tidal stress, for frictional coefficients ranging from 0 to 0.8, for the Olympic Peninsula (a, c) and Vancouver Island (b, d). (a) Olympic Peninsula, August 12-16, 2010. (b) Vancouver Island, August 25 to Sept. 1, 2010. (c) Olympic Peninsula, August 12-16, 2011. (cd) Vancouver Island, August 19 to 29, 2011. For $\mu = 0$, the lag time to maximum cross correlation is (a) -3.25 hours, (b) -2.25 hours, (c) -1.00 hours, (d) -1.75 hours. The lag time for the Olympic Peninsula 2010 is surprisingly large; this may reflect the fact that the time span used is too short to get accurate results. We did not necessarily have a tremor location every 5 minutes in each polygon. In order to accurately assess the time shifts, we averaged the amplitudes in 1 hour windows. When there were no measurements for an hour, we interpolated between the two nearest measurements. Our time windows are limited to times when there was no gap larger than 3 hours.

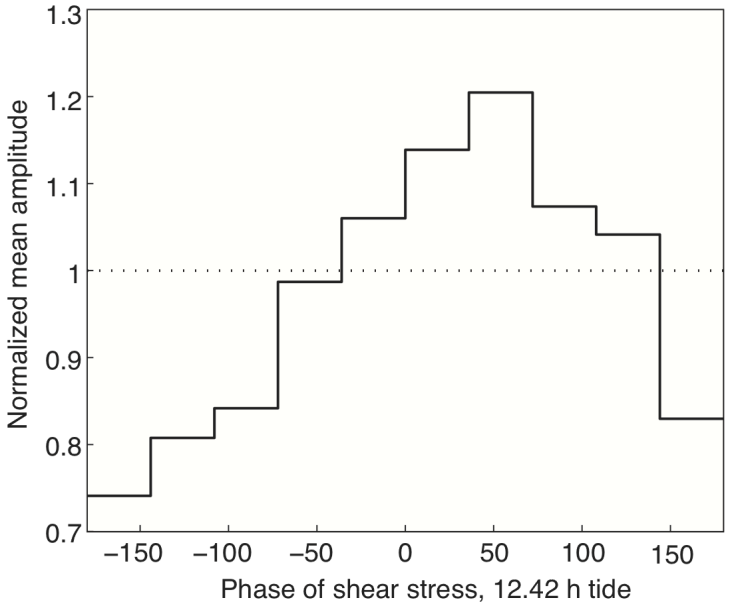

Figure 6. Normalized average tremor amplitude in phase bin compared to phase of the 12.42 hour tide shear stress. The phase-amplitude comparison is done in the Olympic Peninsula and Vancouver Island polygons individually, comparing amplitudes to stress phase at the respective reference point. Then both are averaged together to create this figure. The highest average amplitude occurs around 55°. This bin corresponds to a lead of 1.25 to 2.5 hours. Note that the positive phase shift means that the amplitude is advanced relative to the peak stress.

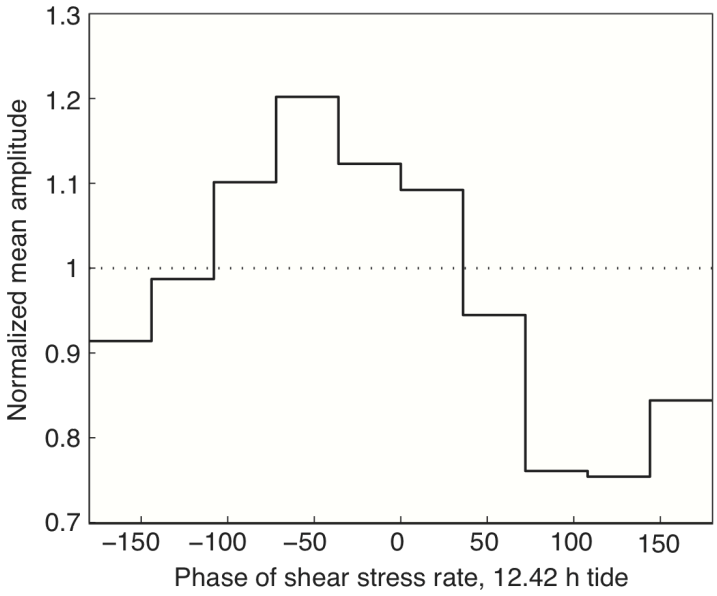

Figure 7. Normalized average tremor amplitude in phase bin compared to phase of the 12.42 hour tide shear stress rate, showing that the maximum tremor amplitude occurs after the peak stress rate. The phase-amplitude comparison is done in the Olympic Peninsula and Vancouver Island polygons individually, comparing amplitudes to stress phase at the respective reference point. Then both are averaged together to create this figure. The highest average amplitude occurs around 55°. This bin corresponds to a lead of 1.25 to 2.5 hours. Note that the positive phase shift means that the peak stress rate precedes the peak amplitude.

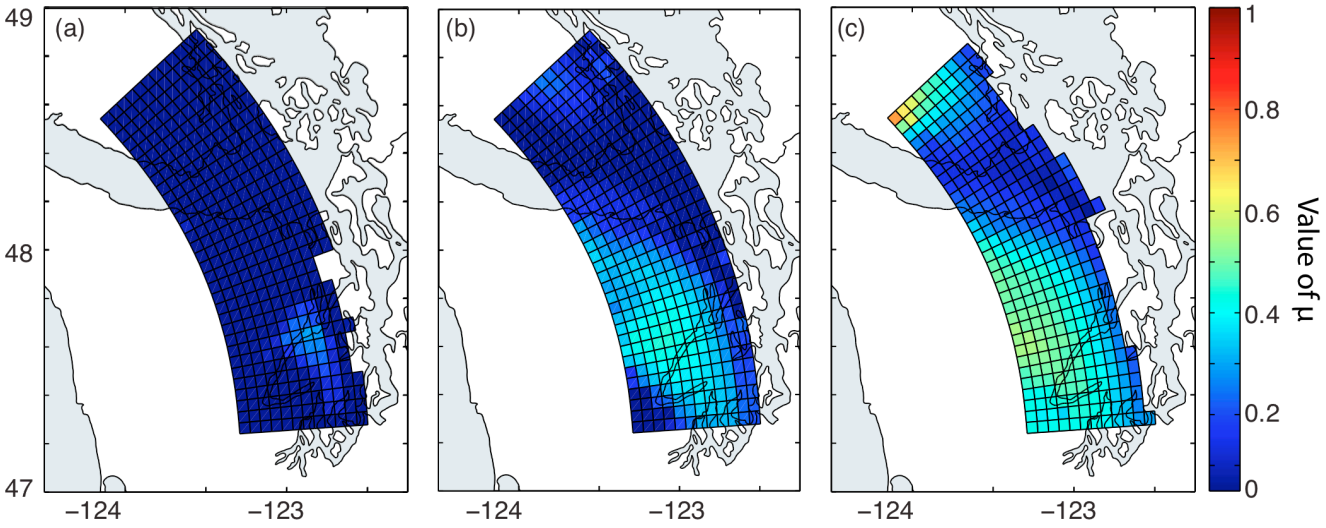

Figure 8. The middle figure (b) shows the value of μ that produces the best correlation between tremor amplitudes and tidal stresses, with tremor amplitudes shifted forward in time by 1.5 hours. The flanking figures show (a) the lower and (b) the upper bounds on μ, defined as the smallest and largest μ values fall within the 95% confidence limits on the "best" μ.

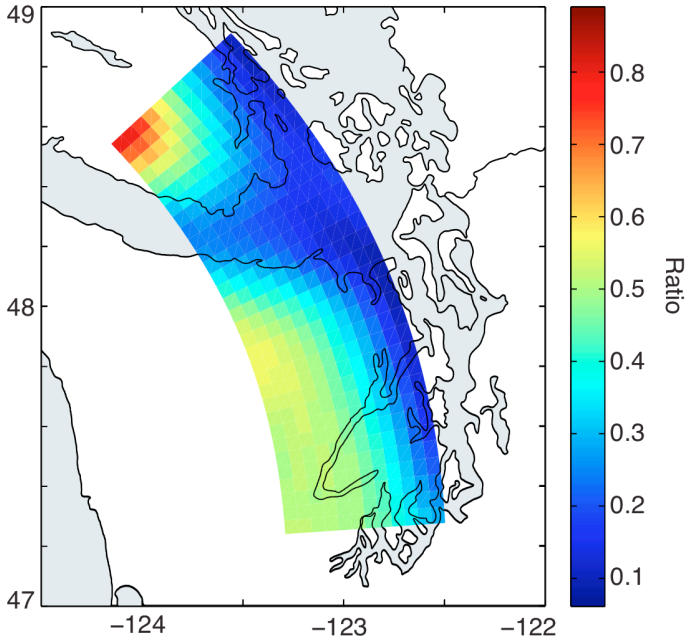

Figure 9. Ratio of the root-mean-square of the shear stress time series to the root-mean-square of the normal stress time series. Over water, the amplitude of the normal stress is 5 to 10 times that of the shear stress, while on land it can be less than twice that of the shear stress.

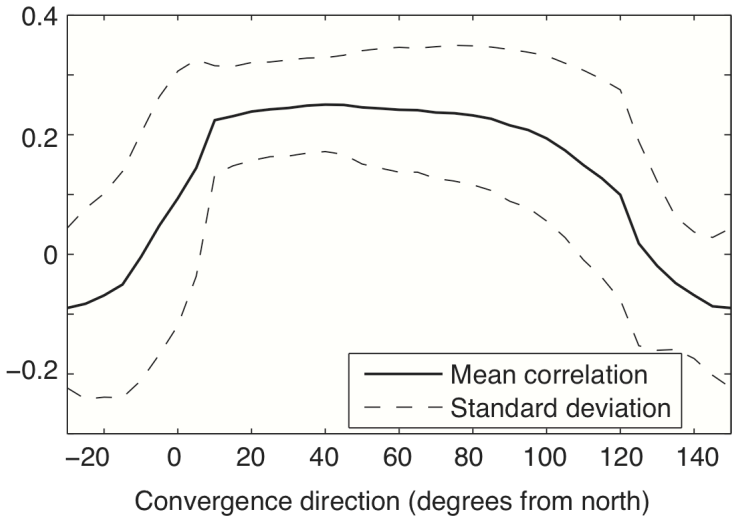

Figure 10. For 180° of convergence directions, this figure shows the mean correlation between tremor amplitude and tidal stress for all the grid points that have at least 40 individual tremor amplitudes. The grid is the same as that shown in Figure 8. The correlation calculation is performed for a Coulomb stress with $\mu = 0.1$ only, and a 1.5 hour time shift is introduced to align peak amplitudes with peak shear stress. (With no time shift, the correlations are slightly lower, but the shape of the curve is the same.) Convergence directions between 10° and 80° from north produce similarly good correlations. Convergence directions less than 10° and greater than 100° produce no correlation or an anticorrelation between tremor amplitudes and tidal stresses.

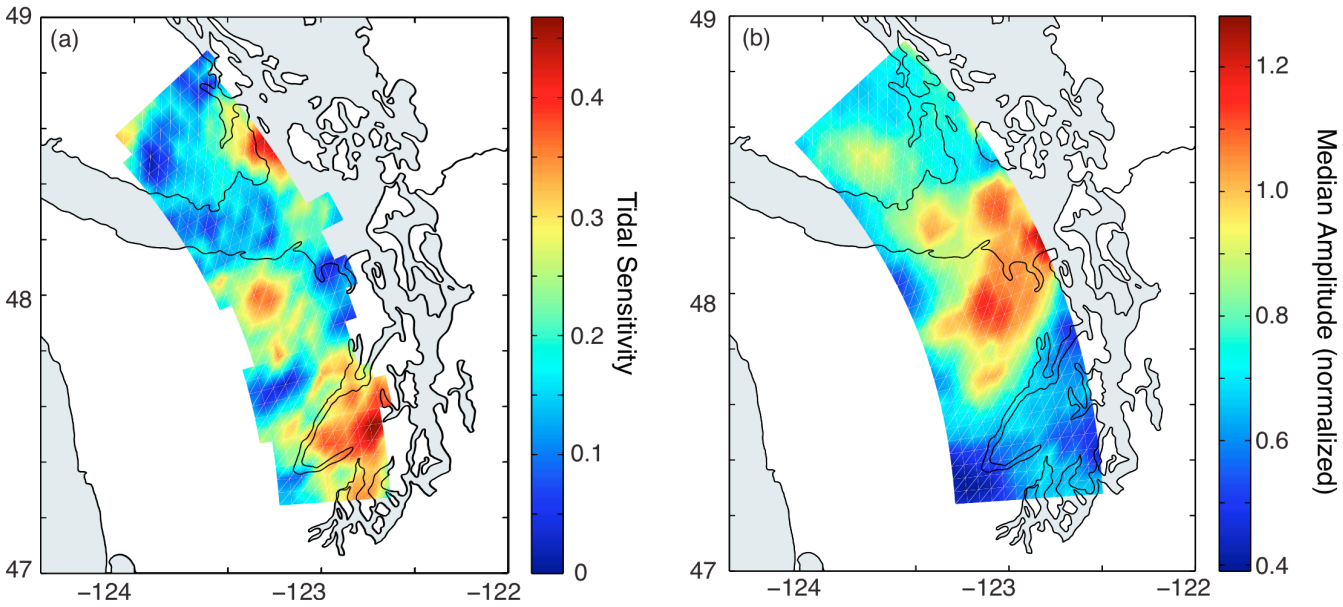

Figure 11. (a) Tidal sensitivity values, based on the method of Ide [2012]. (b) Median amplitudes of the tremor detections used in the sensitivity calculation are shown at right for comparison. The amplitude scale is normalized.

References

Agnew, D. C. (1997), NLOADF: A program for computing ocean-tide loading, *Journal of Geophysical Research*, *102*, doi:10.1029/1096JB03458.

Audet, P., M. Bostock, N. I. Christensen, and S. M. Peacock (2009), Seismic evidence for overpressured subducted oceanic crust and megathrust fault sealing, *Nature*, *457*, 76-78.

Audet, P., M. Bostock, D. C. Boyarko, M. R. Brudzinski, and R. M. Allen (2010), Slab morphology in the Cascadia fore arc and its relation to episodic tremor and slip, *Journal of Geophysical Research*, *115*, B00A16, doi:10.1029/2008JB006053.

Bartlow, N. M., S. Miyazaki, A. M. Bradley, and P. Segall (2011), Space-time correlation of slip and tremor during the 2009 Cascadia slow slip event, *Geophysical Research Letters*, *38*, L18309, doi:18310.11029/12011GL048714.

Brown, J. R., G. C. Beroza, S. Ide, K. Ohta, D. R. Shelley, S. Y. Schwartz, W. Rabbel, M. Thorwart, and H. Kao (2009), Deep low-frequency earthquakes in tremor localize to the plate interface in multiple subduction zones, *Geophysical Research Letters*, *36*, L19306, doi:19310.11029/12009GL040027.

Brudzinski, M. R., and R. M. Allen (2007), Segmentation in episodic tremor and slip all along Cascadia, *Geology*, *35*(10), 907-910.

Dragert, H., K. Wang, and T. S. James (2001), A silent slip event on the deeper Cascadia Subduction Interface, *Science*, *292*, 1525-1528.

Gomberg, J., J. L. Rubinstein, Z. Peng, K. C. Creager, J. E. Vidale, and P. Bodin (2008), Widespread triggering of nonvolcanic tremor in California, *Science*, *319*, 173.

Hawthorne, J. C., and A. M. Rubin (2010), Tidal modulation of slow slip in Cascadia, *Journal of Geophysical Research*, *115*, B09406, doi:09410.01029/02010JB007502.

Hirose, H., and K. Obara (2010), Recurrence behavior of short-term slow slip and correlated nonvolcanic tremor episodes in western Shikoku, southwest Japan, *Journal of Geophysical Research*, *115*, B00A21, doi:10.1029/2008JB006050.

Ide, S. (2010), Striations, duration, migration and tidal response in deep tremor, *Nature*, *466*, 356-359.

Ide, S. (2012), Variety and spatial heterogeneity of tectonic tremor worldwide, *Journal of Geophysical Research*, *117*, B03302, doi:03310.01029/02011JB008840.

Kao, H., and S.-J. Shan (2004), The source-scanning algorithm: mapping the distribution of seismic sources in time and space, *Geophysics Journal International*, *157*, 589-594.

Kao, H., K. Wang, H. Dragert, J. Y. Kao, and G. Rogers (2010), Estimating seismic moment magnitude (Mw) of tremor bursts in northern Cascadia: Implications for the "seismic efficency" of episodic tremor and slip, *Geophysical Research Letters*, *37*, L19306, doi:19310.11029/12010GL044927.

Kao, H., S.-J. Shan, H. Dragert, G. Rogers, J. F. Cassidy, and K. Ramachandran (2005), A wide depth distribution of seismic tremors along the northern Cascadia margin, *Nature*, *436*, 841-844.

Kato, A., S. Sakai, T. Iidaka, T. Iwasaki, and N. Hirata (2010), Non-volcanic seismic swarms triggered by circulating fluids and pressure fluctuations above a solidified diorite intrusion, *Geophysical Research Letters*, *37*, L15302, doi:15310.11029/ 12010GL043887.

La Rocca, M., K. C. Creager, D. Galluzzo, S. Malone, J. E. Vidale, J. R. Sweet, and A. G. Wech (2009), Cascadia tremor located near plate interface constrained by S minus P wave times, *Science*, *323*, 620-623.

Lambert, A., H. Kao, G. Rogers, and N. Courtier (2009), Correlation of tremor activity with tidal stress in the northern Cascadia subduction zone, *Journal of Geophysical Research*, *114*, B00A08, doi:10.1029/2008JB006038.

Maeda, T., and K. Obara (2009), Spatiotemporal distribution of seismic energy radiation from low-frequency tremor in western Shikoku, Japan, *Journal of Geophysical Research*, *114*, B00A09, doi:10.1029/2008JB006043.

McCaffrey, R., A. I. Qamar, R. W. King, R. Wells, G. Khazaradze, C. A. Williams, C. W. Stevens, J. J. Vollick, and P. J. Zwick (2007), Fault locking, block rotation and crustal deformation in the Pacific Northwest, *Geophysics Journal International*, *169*, 1315-1340.

McCrory, P. A., J. L. Blair, D. H. Oppenheimer, and S. R. Walter (2004), Depth to the Juan de Fuca Slab Beneath the Cascadia Subduction Margin— A 3-D Model for Sorting Earthquakes, *U.S. Geol. Surv. Data Series 91*.

Nadeau, R. M., and D. Dolenc (2005), Nonvolcanic tremors deep beneath the San Andreas Fault, *Science*, *307*, 389.

Nakata, R., N. Suda, and H. Tsuruoka (2008), Non-volcanic tremor resulting from the combined effect of Earth tides and slow slip events, *Nature Geoscience*, *1*, doi:10.1038/ngeo1288.

Obara, K. (2002), Nonvolcanic deep tremor associated with subduction in southwest Japan, *Science*, *296*, 1679-1681.

Payero, J. S., V. Kostoglodov, N. Shapiro, T. Mikumo, A. Iglesias, X. Pérez-Campos, and R. W. Clayton (2008), Nonvolcanic tremor observed in the Mexican subduction zone, *Geophysical Research Letters*, *35*, doi:10.1029/2007GL032877.

Peng, Z., and J. Gomberg (2010), An integrated perspective of the cintinuum between earthquakes and slow-slip phenomena, *Nature Geoscience*, *3*, doi:10.1038/NGEO1940.

Preston, L. A., K. C. Creager, R. S. Crosson, T. M. Brocher, and A. M. Trehu (2003), Intraslab earthquakes: deyhydration of the Cascadia slab, *Science*, *302*, 1197-1200.

Rogers, G., and H. Dragert (2003), Episodic tremor and slip on the Cascadia subduction zone: the chatter of silent slip, *Science*, *300*, 1942-1943.

Rubin, A. M. (2008), Episodic slow slip events and rate-and-state friction, *Journal of Geophysical Research*, *113*, B11414, doi:11410.11029/12008JB005642.

Rubinstein, J. L., M. La Rocca, J. E. Vidale, K. C. Creager, and A. G. Wech (2008), Tidal modulation of nonvolcanic tremor, *Science*, *319*, 186-189.

Rubinstein, J. L., J. E. Vidale, J. Gomberg, P. Bodin, K. C. Creager, and S. D. Malone (2007), Non-volcanic tremor driven by large transient shear stresses, *Nature*, *448*, 579-582.

Schmidt, D. A., and H. Gao (2010), Source paramenters and time-dependent slip distributions of slow slip events on the Cascadia subduction zone from 1998 to 2008, *Journal of Geophysical Research*, *115*, B00A18, doi:10.1029/2008JB006045.

Shelly, D. R., G. C. Beroza, and S. Ide (2007), Non-volcanic tremor and low-frequency earthquake swarms, *Nature*, *446*, 305-307.

Shelly, D. R., G. C. Beroza, H. Zhang, C. H. Thurber, and S. Ide (2006), High-resolution subduction zone seismicity and velocity structure beneath Ibaraki Prefecture, Japan, *Journal of Geophysical Research*, *111*, B06311, doi:06310.01029/02005JB004081.

Szeliga, W., T. Melbourne, M. Santillan, and M. Miller (2008), GPS constraints on 34 slow slip events within the Cascadia subduction zone, 1997–2005, *Journal of Geophysical Research*, *113*, B04404, doi:04410.01029/02007JB004948.

Thomas, A. M., R. M. Nadeau, and R. Bürgman (2009), Tremor-tide correlations and near-lithostatic pore pressure on the deep San Andreas fault, *Nature*, *462*, 1048-1051.

Thomas, A. M., R. Bürgman, D. R. Shelly, N. M. Beeler, and M. L. Rudolph (2012), Tidal triggering of low frequency earthquakes near Pakrfield, California: Implications for fault mechanics within the brittle-ductile transition, *Journal of Geophysical Research*, *117*, doi:10.1029/2011JB009036.

Watanabe, T., Y. Hiramatsu, and K. Obara (2007), Scaling relationship between the duration and the amplitude of non-volcanic deep low-frequency tremors, *Geophysical Research Letters*, *34*, L07305, doi:07310.01029/02007GL029391.

Wech, A. G. (2010), Interactive tremor monitoring, *Seismological Research Letters*, *81*(4), 664-669.

Wech, A. G., and K. C. Creager (2007), Cascadia tremor polarization evidence for plate interface slip, *Geophysical Research Letters*, *34*(L22306), doi:10.1029/2007GL031167.
Wech, A. G., and K. C. Creager (2008), Automated detection and location of Cascadia tremor, *Geophysical Research Letters*, *35*, doi:10.1029/2008GL035458,.
Wech, A. G., C. M. Boese, T. A. Stern, and J. Townend (2012), Tectonic tremor and deep slow slip on the Alpine Fault, *Geophysical Research Letters*, *39*, L10303, doi:10310.11029/12012GL051751